PPPL-2056

PPPL-2056

UC20-B,F

ATTAINMENT OF HIGH CONFINEMENT IN NEUTRAL BEAM HEATED DIVERTOR DISCHARGES IN THE PDX TOKAMAK

By

S.M. Kaye et al.

NOVEMBER 1983

PLASMA PHYSICS LABORATORY

PRINCETON UNIVERSITY

PRINCETON, NEW JERSEY

PREPARED FOR THE U.S. DEPARTMENT OF ENERGY,
UNDER CONTRACT DE-AC02-76-CHO-3073.

NOTICE

Printed in the United States of America.

Available from:

National Technical Information Service
U. S. Department of Commerce
5285 Port Royal Road
Springfield, Virginia 22151

Price: Printed Copy $ * ; Microfische $3.50

*PAGES	NTIS Selling Price
1-25	$5.00
26-50	$6.50
51-75	$8.00
76-100	$9.50
101-125	$11.00
126-150	$12.50
151-175	$14.00
176-200	$15.50
201-225	$17.00
226-250	$18.50
251-275	$20.00
276-300	$21.50
301-325	$23.00
326-350	$24.50
351-375	$26.00
376-400	$27.50
401-425	$29.00
426-450	$30.50
451-475	$32.00
476-500	$33.50
500-525	$35.00
526-550	$36.50
551-575	$38.00
576-600	$39.50

For documents over 600 pages, add $1.50 for each additional 25 page increment.

PPPL--2056

DE84 004306

ATTAINMENT OF HIGH CONFINEMENT IN NEUTRAL BEAM HEATED DIVERTOR DISCHARGES IN THE PDX TOKAMAK

S.M. Kaye, M. Bell, K. Bol, D. Boyd (1), K. Brau, D. Buchenauer, R. Budny, A. Cavallo (1), P. Couture (2), T. Crowley, D. Darrow, H. Eubank, R. Fonck, R. Goldston, D. Grek, K. Jaehnig, D. Johnson, R. Kaita, H. Kugel, B. LeBlanc (3), J. Manickam, D. Manos, D. Mansfield, E. Mazzucato, R. McCann, D. McCune, K. McGuire, D. Mueller, A. Murdock (1), M. Okabayashi, K. Okano (4), D. K. Owens, D. Post, M. Reusch, G. Schmidt, S. Sesnic, R. Slusher (5), S. Suckewer, C. Surko (5), H. Takahashi, F. Tenney, H. Towner, J. Valley (5)

Plasma Physics Laboratory, Princeton University

Princeton, N.J. 08544

(1) University of Maryland, College Park, Maryland.
(2) Institut de Recherche d'Hydro-Quebec, Varennes, Que, Canada
(3) INRS-Energie, Que, Canada
(4) University of Tokyo, Tokyo, Japan
(5) Bell Laboratories, Murray Hill, New Jersey 07974

Abstract

The PDX divertor configuration has recently been converted from an open to a closed geometry to inhibit the return of neutral gas from the divertor region to the main chamber. Since then, operation in a regime with high energy confinement in neutral beam heated discharges (ASDEX H-mode) has been routine over a wide range of operating conditions. These H-mode discharges are characterized by a sudden drop in divertor density and H_α emission and a spontaneous rise in main chamber plasma density during neutral beam injection. The confinement time is found to scale nearly linearly with plasma current, but it can be degraded due to either the presence of edge instabilities or heavy gas puffing. Detailed Thomson scattering temperature profiles show high values of Te near the plasma edge (~ 450 eV) with sharp radial gradients (~ 400 eV/cm) near the separatrix. Density profiles are broad and also exhibit steep gradients close to the separatrix.

I. INTRODUCTION

In the first three years of its operation, the divertor of the PDX tokamak was configured in an open geometry in which neutrals from the divertor region had fairly unobstructed access to the main chamber. Such operation produced very clean discharges during ohmic heating and had favorable power handling characteristics, especially at high densities, during neutral beam injection (NBI).[1] However, this configuration did not allow operation in a high recycling divertor regime, described in[2] and observed in ASDEX and DIII,[3-6] in which the power flow to the neutralizer plates could be strongly reduced. Because of this consideration the PDX divertor was modified extensively in late 1982 to allow operation in this high recycling regime. During ensuing operation, PDX routinely achieved plasmas during neutral beam injection (NBI) with the characteristics of the H-mode discharges first observed in the ASDEX tokamak.[7-9] The energy and particle confinement of these plasmas were substantially better than that of beam heated plasmas in the open configuration. High confinement plasmas have also been reported in the DIII tokamak.[10,11] An especially important feature of the PDX facility is the near perpendicular neutral beam injection system of the joint PPPL-ORNL Heating Project which provided power levels up to 6 MW with deuterium injection for beam pulse lengths up to 300 msec, enabling exploration of the H-mode phenomenon at higher injected beam powers than heretofore reported. A complete description of PDX may be found in Meade et al.,[12] and a description of the PDX neutral injection system is given in Kugel et al.[13] A detailed description of H-mode plasmas is made possible by a full complement of high resolution diagnostics of the main, edge, and divertor plasmas. This paper describes the changes made in the PDX hardware which allowed operation in the closed divertor configuration. Characteristics of neutral beam heated plasmas

are described with particular emphasis on the properties of H-mode type plasmas. Confinement, transport, and fluctuation characteristics are presented with the goal of delineating the properties of the divertor operation that lead to H-mode plasmas.

II. DIVERTOR HARDWARE AND OPERATION MODIFICATIONS

The unmodified divertor configuration allowed neutrals from the divertor region easy access to the main chamber via the outer divertor region which contained no plasma (Figure 1a). With extensive titanium gettering in both divertor chambers, a relatively low neutral gas pressure was usually obtained in the divertor region.[14] Because no pressure difference between the main chamber and the divertor could be maintained, high density operation with NBI led to high pressures ($>10^{-3}$ Torr) in the main chamber as well as in the divertor region.[1] Divertor operation was continually plagued by shorts between the titanium neutralizer plates and other machine components, and by excessive bursting of titanium radiation, presumably due to arcing from titanium liners and/or divertor region. More importantly, this divertor configuration made it quite difficult to startup the discharge and entirely precluded operation with $I_p > 400$ kA.

In the modified configuration (Figure 1b), the opening between the outer divertor coils and the main chamber was closed. The titanium liners and neutralizer plates were replaced with stainless steel components owing to the better thermal properties of steel, and the neutralizer support and electrical insulation assembly was entirely redesigned to reduce the occurrence of shorts between the plates and other machine components. Finally, the outer divertor coils were taken out of the divertor field circuit which allowed easier discharge startup, due to the reduction of field gradients in the outer

region, and attainment of discharges with $I_p \lesssim 500$ kA. These modifications, along with restricting gettering to the lower dome, also eliminated the metallic impurity bursting.

For most of the operating period to be discussed here, D° discharges were run in a single null configuration. This was accomplished by displacing the plasma 3 to 4 cm above the midplane so that the plasma was connected primarily to the upper, non-gettered dome. The disconnection to the lower divertor was verified by microwave interferometer measurements of plasma density in the lower and upper chambers. The plasma behavior, even in ohmic discharges, was dramatically different than it had been earlier because of the hardware and operation changes. High neutral gas pressures of up to 8×10^{-4} Torr were obtained in the upper divertor chamber with a compression ratio of up to 30 between the divertor and main plasma chambers.[15] In addition, a greatly reduced power flow to the divertor plates was observed during NBI in the closed configuration relative to that in the open configuration. Only 10% of the absorbed power was deposited on the neutralizer plates, indicating a plugging of the divertor scrape-off to this energy flow.[16]

III. DISCHARGE CHARACTERISTICS WITH NEUTRAL BEAM INJECTION

The general behavior of PDX NBI discharges in the closed divertor configuration is similar to that described by the ASDEX group.[4,5] Above a threshold in absorbed power, a spontaneous rise in τ_E, τ_p, and $\bar{n}_e$ occurred as the discharge evolved from a low-confinement (pre-transition) phase to a high-confinement (H) phase. Characteristics of a discharge exhibiting the transition into the H-mode are shown in Figure 2. In this particular discharge, a steady gas feed rate (20 to 30 Torr-l/s) from 300 to 600 msec, using two valves in the upper dome separated toroidally by 180°, was

used. The transition into the H-phase at 450 msec is seen from an abrupt change in the rate of rise of the main chamber plasma density (upper left panel), with no modification of the external gas feed rate, and by a rapid drop in the divertor H_α emission (upper right panel). In this paper, "H_α" emission is used to denote the combined H_α/D_α emission. This sharp drop in the divertor H_α signal was used as a criterion to determine whether or not the plasma had experienced a transition into the H-phase. In the H-phase the level of toroidally averaged main chamber H_α emission (lower left panel) remained nearly constant, and the divertor line density (lower right panel) exhibited behavior similar to that of the divertor H_α emission, dropping suddenly at the transition.

The transition into the H-phase usually, but not always, occurred at the fall of a sawtooth oscillation, as determined from the soft X-ray emissivity measurements, and typically required > 1.6 MW of absorbed beam power. A few instances of transitions with $P_{abs} \sim 1$ MW were observed. After the transition into the H-phase, the sawtooth amplitude was seen to decrease by as much as 50%. The sawtooth period in the H-phase remained constant or increased. Transitions were observed to occur anywhere from 10 to 200 msec after the onset of NBI, with the later transitions associated with higher toroidal field and/or lower plasma density, and thus lower beam power.

The rise in plasma density at the time of the transition, coupled with constant main chamber H_α emission and a measured 30-50% decrease in fast neutral efflux from the plasma core, indicates an improvement in particle confinement time by as much as a factor of 2 at the transition. In addition, the nearly constant level of main chamber H_α emission, despite the rising plasma density, indicates little change with time of the ionization source rate at the midplane. This also implies that the particle confinement had

increased across the transition. Total bolometrically measured power loss from the discharge did not change substantially across the transition into the H-phase. Spectroscopic measurements show a decrease in central radiation at the transition and some increase in edge radiation.[16] Z_{eff} deduced from visible bremsstrahlung and plasma resistivity was found to decrease continuously with time through the NBI phase of the divertor discharges, going from Z_{eff}=4 at the start of NBI to values of 2 to 2.5 well into the H-phase. The decrease in Z_{eff} is due to the increasing density and not to an increase in impurity content.[16]

An effect seen in most PDX H-phase discharges is the spiky behavior of the H_α (main chamber and divertor) emission and the divertor line density (Figure 2). The presence of the H_α spikes, which appear only in the H-phase, has a deleterious effect on particle and energy confinement, resulting in a clamp on the density rise and a degradation of energy confinement time. The nature of these fluctuations will be discussed in more detail later.

Figure 3 presents the time evolution of several additional discharge parameters. In this discharge, 2.3 MW of D^o power was injected into a D^+ plasma during the current rise. After the onset of NBI, the plasma density, measured by the 2 mm microwave interferometer, remained constant in time (upper right panel), and the total equilibrium energy confinement time determined from magnetic equilibrium measurements (lower right panel) was calculated to be 30 msec. The total equilibrium energy confinement time is defined to be

$$\tau_E^{eq} = \frac{W}{P_{abs} - \frac{\partial W}{\partial t}} ,$$

where P_{abs} is the neutral beam power ionized in the plasma. The total stored energy, W, is determined from the measured $\ell_{i/2} + \beta_{pol}$ signal and from an estimated current profile $(J \alpha (1 - (r/a)^2)^{(q_a/q_o - 1)}, q_o = 0.8)$. Based on comparisons between the results of this simple model for τ_E^{eq} and those with the more sophisticated beam model in the full kinetic transport analysis code, the accuracy of the magnetics τ_E^{eq} is estimated to be ± 15%. At 470 msec, the plasma density suddenly and continuously rose to a peak value of 4×10^{13} cm-3 with no adjustment to the gas feed. For this discharge a steady feed from the two upper dome valves from 80 to 600 msec was used. At this transition time of 470 msec, the loop voltage dropped (upper left panel), the $\ell_i/2 + \beta_{pol}$ and $\langle\beta_T\rangle$ (determined from the former quantity) began to increase at a faster rate, and the total energy confinement increased rapidly to a value of 46 msec.

H-mode plasmas were observed over a wide range of parameter space in PDX (I_p=210 to 490 kA, B_t=0.9 to 2.1 T, $\bar{n}_e$ = 1.5 to 7 × 10^{13} cm^{-3}, P_{inj}=1 to 5.5 MW, β_{pol}=0.4 to 1.4, $\langle\beta_T\rangle$=0.3 to 2.4%). In particular, we found no lower limit on q_{shaf} for attaining the H-mode. Here, q_{shaf} is taken to be the cylindrical q value for an equivalent circular plasma, taking into account toroidal corrections $\left(q_{shaf} = \left(aB_T/RB_p\right) \cdot \left[1 + a^2/R^2 \left(1 + (\ell_i/2 + \beta_{pol})^2/2\right)\right]\right.$. Values of q_{shaf} as low as 2.05 have been achieved during H-mode plasmas.

The H_α spikes, which correlated with a reduction in confinement, were identified by the soft X-ray array as edge relaxation phenomena (ERP's) because of their sawtooth-like structure in the outer plasma. The top trace in Figure 4a is the divertor H_α emission on an expanded time scale, and three large H_α spikes are clearly observed. The second trace in Figure 4a is a Mirnov coil signal and represents the magnetic fluctuation amplitude in the plasma. While the first H_α spike was not associated with oscillatory MHD

activity, the later two were accompanied by bursting m=1 activity. This MHD was identified as low amplitude fishbone activity[17] in the plasma core by the soft X-ray signals shown in Figure 4b. The Mirnov loop signature of the ERP alone, on this time scale, was a very sharp spike as seen in Figure 4a. At high values of $\langle\beta_T\rangle q$, the ERP's and fishbones tended to become closely coupled together in time. The X-ray signal at the plasma edge, clearly associated with the H_α spikes, shows a sawtooth-type inversion at r=40 cm. An m=3/n=1 precursor mode to the ERP's with a large growth rate could sometimes be identified within the sharp Mirnov spike. This precursor mode may be indicative of a surface kink mode perturbation. Theoretical analysis indicates that these discharges were potentially unstable to surface kinks, due to their substantial edge current density, unlike the high-$\langle\beta_T\rangle$ limiter plasmas studied previously in PDX.[18] The occurrence of the internal kink (fishbone) mode along with the resultant beam ion loss at high values of $\langle\beta_T\rangle q$, with the near perpendicular NBI on PDX, indicates that the H-mode phenomenon will not aid the attainment of high-$\langle\beta_T\rangle$ values beyond those achieved in limiter discharges.

Differences between L and H-phase plasmas are seen also in higher frequency density fluctuations. Data from the 2 mm microwave scattering experiment indicated that the relative fluctuation level, $\tilde{n}/\bar{n}_e$, near the center of the plasma decreased across the transition into the H-phase, owing to the increase in plasma density. Results from the CO_2 scattering experiment indicated that during the H-phase a significant fraction of the fluctuation level at the plasma edge resided in a quasi-coherent mode. This mode, unique to the H-phase, occurred anywhere from 30 to 100 kHz in bursts of 10 to 20 cycles, repeating every 0.2 to 1 msec, and it was observed to grow within 5 msec after the transition.

A striking difference between the pre-transition plasmas and those well into the H-phase is seen in Figure 5. The top portion of the figure shows the electron temperature and density profiles measured by the 56-point Thomson scattering system in a pre-transition plasma, and the bottom portion shows the corresponding profiles ~ 100 msec after the transition. For the data shown, R_0=140 cm and a=39 cm on the basis of magnetics measurements. In the pre-transition plasma both the T_e and n_e profiles were quite symmetric and exhibit low values of temperature (100 to 150 eV) and density ($\sim 7 \times 10^{12}$ cm^{-3}) near the plasma edge. At the transition into the H-mode, the central T_e value typically dropped, and the edge T_e rose several hundred eV; however, in time the central T_e recovered to at least its pre-transition level, while the edge remained hot. Little change was seen in the central density at the transition; the edge density rose first, with the central portion of the profile filling in 30 to 50 msec later. Consequently, well into the H-phase (Figure 5b), both profiles have developed well-defined pedestals with edge T_e values of up to 450 eV and edge densities of 1.5×10^{13} cm^{-3}. Note that the temperature gradient within the plasma has changed very little between the two profiles. The large gradients are seen at the plasma edge for both temperature and density.

The detailed temperature and density profiles in the midplane edge region were measured using a single point Thomson scattering system. Such data is crucial to understanding the plasma transport in the edge region. The edge T_e and n_e profiles are plotted as a function of major radius in Figure 6. The points inside 180 cm were obtained from the multi-point Thomson scattering system, with the remainder measured by the single point system. Efforts are underway to locate accurately the position of the separatrix using the measured pressure profiles as input to a magnetic equilibrium code. While

the T_e and n_e profiles show no features in the vicinity of the separatrix in the pre-transition phase, the large gradients appear during the H-phase near the separatrix. With temperatures inside the separatrix of ~ 450 eV, the gradient very near to the separatrix and possibly actually on open field lines is 400 eV/cm. The local depression in the n_e profile at R=182 cm may be due to the pumping action of the lower divertor. Measurements from a triple Langmuir probe in the divertor region near the outside neutralizer plates indicate a 50% drop in temperature across the profile going from pre-transition to H-phase, with temperatures of 20 eV at the separatrix during the H-phase. Further details on the divertor measurements can be found in.[19] During discharges with ERP's (not shown), the temperatures just inside the separatrix are reduced to values of 200 to 250 eV, and the gradients in both T_e and n_e broaden, with a corresponding increase in cross-field power flow as measured by a mid-plane calorimeter/probe.[20] ERP's tend to reduce T_e across the profile in the divertor region and result in broader T_e and n_e profiles there as well. Estimates of classical parallel heat conduction loss indicate that if the midplane edge gradient resides on open field lines, the temperature difference along the field line of at least ~ 300 eV between the midplane and divertor region would be impossible to maintain in the absence of an additional mechanism to impede heat flow.[21]

IV. TRANSPORT ANALYSIS

The main plasma Thomson scattering T_e and n_e profiles shown in Figure 5 were used as a basis to study the plasma transport in H-mode discharges using the TRANSP transport analysis code.[22,23] A time-evolving description of the divertor discharges was obtained by concatenating Thomson scattering profiles taken during a set of reproducible discharges. The results of several of

these full analyses indicate that electron thermal conduction was the dominant power loss in all phases of the NBI discharge.

The deduced χ_e during the pre-transition and H-phases for one fully analyzed divertor discharge is shown in Figure 7. A 30-50% reduction in χ_e across the entire profile and especially near the edge is noted. The major source of uncertainty in the deduced χ_e's are from errors in the measured T_e profiles. Systematic errors in T_e of ± 20%, much larger than the random errors shown in Fig. 5, propagate into a factor of 1.5 to 2 uncertainty in χ_e. However, the same data handling techniques were used for both the pre-transition and H-phase T_e profiles; therefore, the systematic improvement in χ_e over the entire profile is believed to be statistically significant. Because the temperature gradients and conduction power loss changed very little across the transition, the improvement in the deduced χ_e is due to the increased plasma density. In typical L-mode plasmas this is not observed; when the density is increased by increasing the gas feed, T_e drops about in proportion to the density rise so that χ_e is unchanged. We do not necessarily deduce from the H-mode data that $\chi_e \propto 1/n_e$, but rather that improved confinement results in both a drop in χ_e and a correlated increase in density. While the pre-transition χ_e near the plasma edge was found to be comparable to Bohm diffusivity, during the H-phase the deduced χ_e in the modest gradient region was found to be 1/5 of Bohm, due to both the increased edge T_e (increasing Bohm) and the improvement in the deduced χ_e. The deduced χ_e is still two to three orders of magnitude greater than that predicted by classical theory.

The edge T_e and n_e profiles shown in Figure 6 can be used to estimate an upper limit to the cross-field thermal diffusivities in the region of strong gradients. This is done by assuming that there is no parallel loss or

additional radiative loss in this region, so that all the transport power leaving the main plasma is lost through cross-field conduction in the edge region. In this simplified analysis, the convective cross-field heat losses are ignored. This is consistent with an "upper-limit" estimate to χ_e . In the TRANSP analysis of the main plasma data, $P_{conduction}$ (a) = 3.5 x $P_{convection}$ (a). It is seen from Figure 6 that in the pre-transition phase, the temperature gradient and density change very little with major radius. Consequently, this upper limit $\chi_{e\perp}$ is similar to that just inside the plasma, comparable to Bohm diffusivity as discussed. This is typical of many divertor plasmas.[24] The estimate in the H-phase is a bit more difficult to make because of the sharp drop in density. Taking an average density on the gradient, and noting that $\partial T_e/\partial_r$ increases by a factor of 15 from that in the main plasma, we estimate the upper limit $\chi_{e\perp}$ in the strong gradient region in the H-phase to be 10 to 20% of that inside the main plasma. The $\chi_{e\perp}$ in the gradient region then would be only 1/25 of Bohm, but still much higher than classical. Of course, farther out where the temperature gradient is reduced and the density is low, $\chi_{e_\perp}$ will be greater.

V. CONFINEMENT SCALING

The total energy confinement time in the H-mode discharges was found to have little dependence on toroidal field, but it was found to scale nearly linearly with plasma current, in agreement with the result observed on ASDEX and DIII.[25,9] For the highest confinement cases, $\tau_E^{eq} \propto I_p/8\text{-}10$, where τ_E^{eq} is measured in msec and I_p in kA. Although confinement time had no apparent explicit dependence on plasma density, excessive gas puffing and the associated increase in main chamber neutral pressure led to a degradation in confinement. Figure 8 shows confinement times plotted against main chamber

neutral pressure for a set of discharges at I_p=400 kA and B_t=1.6T. The variation in P_{main} from $3x10^{-6}$ to $3x10^{-3}$ Torr was obtained by shot to shot variations in the vertical position of the plasma and gas feed valve (divertor and mid-plane valves). For comparison, midplane pressures of 1 to 2 $x10^{-5}$ Torr were observed in previous limiter discharges.[14] The poorer confinements shown in Figure 8 were typical of discharges positioned vertically on the mid-plane and with gas feeds through the midplane valves. Later experiments with a constant vertical position of 3 to 4 cm above the midplane, and using only dome gas valves, indicated a similar degradation in confinement with increasing P_{main}. In these cases the midplane pressure increased due to increasing gas feed rate. The lowest midplane pressure cases in Figure 8 corresponded to midplane/divertor gas compression ratios of ~30.[15]

Since it was clear that high gas feed rates and the associated increase in main chamber neutral pressure led to confinement degradation, measurements were made to study this degradation for discharges in which the density was forced from $2.5x10^{13}$ cm^{-3} to a value of $5x10^{13}$ cm^{-3} by puffing gas at a rate of 150 Torr-l/s into the discharge 100 msec after the onset of NBI (which corresponded to 30 msec after the transition into the H-mode). Associated with the large gas feed rate was a large increase in midplane H_α emission and divertor density. The midplane H_α signal now tracked the divertor H_α signal, indicating that neutral gas was "blowing through" the divertor throat. Plasma and edge T_e and n_e profiles for this "blow-through" experiment are shown in Figures 9a and 9b, and several major differences can be seen between these data and the profiles shown in Figure 5. The first is that increasing the gas feed rate led to a cooling of the edge to values of 200 eV, only 50 eV higher than is typically seen in the pre-transition phase. Central temperatures were also reduced. The plasma density is higher over the entire

profile and exhibits a clear outward asymmetry. The outward asymmetry seen in the density profile is real and is a feature also observed in many of the standard H-phase profiles. Work to define the source of this asymmetry is presently underway. Both the density and temperature gradients in the edge region are broader. The divertor triple probe measurements during the blow-through indicate that the divertor electron and power density had increased by a factor of ten relative to standard H-phase divertor values, and that the profiles were relatively flat across the scrape-off. The divertor temperature profiles were flat at 12 eV.[19] A spatially resolved measurement of the H_α emission was made using the Thomson scattering spectrometer optics set up to view the upper region of the main chamber which includes the divertor neutralizer plates. The results are plotted in Figure 10 for the standard H-mode and two-beam blow-through case. Also shown is a typical field of view of one of the 56 Thomson scattering channels. During the H-phase, the H_α emission was seen to have two distinct peaks, one peak on either side of the divertor throat near the neutralizer plates, indicating a strong localization of recycling to this divertor region. During the blow-through, the H_α emission increased by a factor of five to ten across the entire viewing area, and the two distinct H_α peaks coalesced into one large emission region, with three times the amplitude, in the vicinity of the x-point. This blow-through result indicates a delocalization of recycling and plasma fueling.

Because confinement was found to scale nearly linearly with I_p, it is useful to define a discharge quality factor, τ_e^{eq}/I_p, in units of msec/kA, in which the linear dependence of τ_e^{eq} on I_p is removed. This enables us to examine the quality of the H-phase confinement as a function of total power ($P_{abs}+P_{oh}$). This parameter is plotted as a function of P_{tot} in Figure 11. For comparison, the gray-shaded region in the plot defines the range of

τ_e^{eq}/I_p from previous $D^o \rightarrow H^+$ limiter discharges.[18,26] All divertor discharges in the figure with $P_{tot}>1.5$ MW exhibited transitions into the H-phase, as defined by the drop in divertor H_α emission, although only discharges at the two beam level (P_{tot}=1.8 to 2.8 MW) had high confinement times. The highest total equilibrium confinement time was determined to be 55 msec at I_p=400 kA, corresponding to a thermal confinement time of >60 msec and an electron energy confinement time of 40 msec at r/a=0.5. Thermal and electron energy confinement times are calculated in the TRANSP transport analysis code, taking into account the stored energy and power input to the thermal plasma only.

All the points plotted in Figure 11 were taken from discharges with co-injection. The highest values of τ_e^{eq}/I_p were from discharges with no ERP's and with no evidence of blow-through, as indicated by low H_α emission levels in the main chamber. The best counter-injection discharges exhibited H-phase plasmas with τ_e^{eq}/I_p nearly as high as the highest co-injection cases, even with a calculated 50% of the injected power being lost on bad orbits; however, often the counter-injection plamas contained large amounts of iron and were consequently either quite disruptive or dominated by central core radiation.

The continuum to low τ_e^{eq}/I_p at the two beam level in Figure 11 is due to discharges with either ERP's or large gas feed rates. At higher powers, τ_e^{eq}/I_p is degraded, the reduction in confinement due again to the presence of ERP's and/or the large gas feed rate necessary to ensure a nondisruptive discharge. To test whether gas feed alone was enough to cause confinement degradation in the ERP-free discharges, an experiment was performed in which the same gas feed rate (150 Torr-l/s) was used in both two-beam and four-beam discharges. The result was that the confinement was found to be low and about equal (τ_e^{eq}/I_p=0.07 to 0.09 msec/kA) for the two power levels, indicating that the large gas feed alone could account for the poorer confinement.

It is seen in the figure that for the previous $D^o \rightarrow H^+$ limiter case $\tau_e^{eq}/I_p = 0.03$ to 0.05 kA/msec for $P_{tot} > 3.5$ MW. Although no systematic studies of isotope effects on energy confinement were made on PDX, the ASDEX group reports confinement times a factor of ~ 1.4 higher for D^+ plasmas than for H^+ plasmas.[25] The difference in confinement times for the $D^o \rightarrow H^+$ limiter and the $D^o \rightarrow D^+$ divertor results at the three and four-beam levels in PDX can be explained, then, by just taking into account a ~ 40% improvement in confinement of D^+ over H^+ plasmas.

VI. CONCLUSIONS

In conclusion, plasmas with improved energy and particle confinement times were routinely achieved with the closed PDX divertor configuration over a wide range of operating conditions. Significant reductions in power flow to the divertor neutralizer plates and increases in gas compression ratio were observed after the conversion to the closed divertor geometry. Confinement improved over that in the L-phase because of the additional stored energy due to T_e and n_e pedestals and because of the reduced electron thermal diffusivities over the entire plasma and especially near the edge. Confinement times were found to scale nearly linearly with plasma current and improved with reduced main chamber neutral pressure. The edge conditions appear to be the key to good H-mode confinement. Although there appears to be a need to keep neutrals from the main plasma to attain high confinement times, H-phase discharges with good confinement exhibited neutral gas pressures that were comparable to those in previous limiter discharges. Consequently, it is not just the low main chamber pressure, but rather this low pressure coupled with other properties of divertor operation that are, as yet, undefined that leads to the edge conditions crucial to good H-mode confinement. Confinement

was found to have little dependence on $\bar{n}_e$ except for the role that excessive gas puffing had in modifying the edge conditions, and it was also found to degrade, also due to edge relaxation phenomena.

The PDX project was supported by the United States Department of Energy Contract No. DE-AC02-76-CHO-3073.

REFERENCES

[1]R. Fonck et al., J. Nucl. Mater. 111 & 112, 343 (1982).

[2]M. Petravic et al., Phys. Rev. Lett. 48, 326 (1982).

[3]ASDEX Team, presented by M. Keilhacker, at the IAEA Technical Meeting on Divertors and Impurity Control, Garching bei München (1981) p. 58.

[4]W. Englehardt et al., J. Nucl. Mater. 111 & 112, 337 (1982).

[5]M. Nagami et al., ibid, 111 & 112, 362 (1982).

[6]M.A. Mahdavi et al., ibid, 111 & 112, 355 (1982).

[7]F. Wagner et al., Phys. Rev. Lett. 49, 1408 (1982).

[8]F. Wagner et al., IPP III/78, June 1982.

[9]F. Wagner et al., in Proceedings of the Ninth IX Conference on Plasma Physics and Controlled Nuclear Fusion Research, Baltimore, 1982, Vol. I., p. 43.

[10]N. Ohyabu et al., in Proceedings of the IEEE International Conference on Plasma Science, San Diego, Cal., 1983 (to be published).

[11]M. Nagami et al., GA-A17056, May 1983.

[12]D. Meade et al., in Proceedings of the Eighth International Conference on Plasma Physics and Controlled Nuclear Fusion Research, Brussels, 1980 (IAEA, Vienna, 1981) Vol. I, p. 665.

[13]H. Kugel et al., Princeton Plasma Physics Laboratory Report No. PPPL-1728, 1981.

[14]H.F. Dylla et al., J. of Nucl. Mater. 111 & 112, 211 (1982).

[15]H.F. Dylla et al., Presented at the Symposium on Energy Removal and Particle Control in Toroidal Fusion Devices, Princeton, NJ, 1983.

[16]M. Bellet al., Presented at the Symposium on Energy Removal and Particle Control in Toroidal Fusion Devices, Princeton, NJ, 1983.

[17]McGuire, K. et al., Phys. Rev. Lett. 50, 891 (1983).

[18]D. Johnson et al., in Plasma Physics and Controlled Nuclear Fusion Research, 1982 (IAEA, Vienna 1983), Vol. I, p. 9.

[19]D.K. Owens et al., Presented at the Symposium on Energy Removal and Particle Control in Toroidal Fusion Devices, Princeton, NJ, 1983.

[20]R. Budny and D. Manos, Presented at the Symposium on Energy Removal and Particle Control in Toroidal Fusion Devices, Princeton, NJ, 1983.

[21]T. Ohkawa et al., GA-A17082 (1983).

[22]R. Hawryluk, Proceeding Course on Physics of Plasmas Close to Thermonuclear Conditions, Report EUR FU RU/XII/476/80, Vol. 1, p.19.

[23]R. Goldston et al., J. Comput. Phys. 43, 61 (1981).

[24]J. Hugill, Nucl. Fus. 23, 331 (1983).

[25]F. Wagner et al., IPP III/86, March 1983.

[26]R. Hawryluk et al., Phys. Rev. Lett. 49, 326 (1982).

FIGURE CAPTIONS

FIG. 1 Flux plots for the unmodified (1a) and modified (1b) PDX divertor geometry.

FIG. 2 Discharge characteristics of a two-beam (~ 2.3 MW) divertor plasma with I_p = 350 kA, B_T = 1.7 T. The transition into the H-phase occurs at 450 msec.

FIG. 3 Further characteristics of a two-beam divertor discharge taken from a D-D confinement analysis (B_T = 1.8 T). The transition occurs at 470 msec.

FIG. 4a $H\alpha$ emissions from the dome region of the divertor chamber (arb. units) and magnetic fluctuation amplitude as measured by a Mirnov coil on the outside midplane of the torus for a ~ 2.3 MW discharge. 4b) Soft X-ray emissivity signals from horizontal chords from an H-phase showing edge relaxation phenomena and m=1 activity in the plasma core.

FIG. 5a Electron temperature and density profiles measured by the 56-point Thomson scattering system in a pre-transition plasma (P_{inj} = 2.3 MW). 5b) Same as 5a for a plasma well into the H-phase (I_p = 400 kA, B_T = 1.8 T).

FIG. 6 Edge electron temperature and density profiles for a pre-transition (open points) and H-phase (solid points) plasma. The

points inside of R=180 cm were measured by the multi-point Thomson scattering system and the rest were measured by the single point Thomson scattering system. The data was taken during a reproducible set of discharges with I_p = 400 kA, B_T = 1.8 T, and P_{inj} = 2.0 MW.

FIG. 7 Electron thermal diffusivities deduced from the TRANSP transport analysis code.

FIG. 8 Total equilibrium confinement time versus main chamber neutral pressure for I_p=400 kA, B_t=1.6 T discharges.

FIG. 9a Multi-point Thomson scattering and 9b) single-point edge Thomson scattering measurements of the electron temperature and density during a two-beam (2.2 MW) blow-through discharge (I_p = 400 kA, B_T = 1.8 T).

FIG. 10 Spatially resolved divertor H_α emission measured by the multi-point Thomson scattering spectrometer during two-beam standard H-mode and blow-through discharges. Also shown is a typical field of view of one of the 56 channels.

FIG. 11 Discharge quality factor, τ_e^{eq}/I_p, versus total power ($P_{abs}+P_{oh}$) for PDX divertor discharges. The gray shaded region is the envelope of discharge quality factors determined for previously measured $D^o \rightarrow H^+$ limiter discharges without ion loss due to fishbone oscillations.

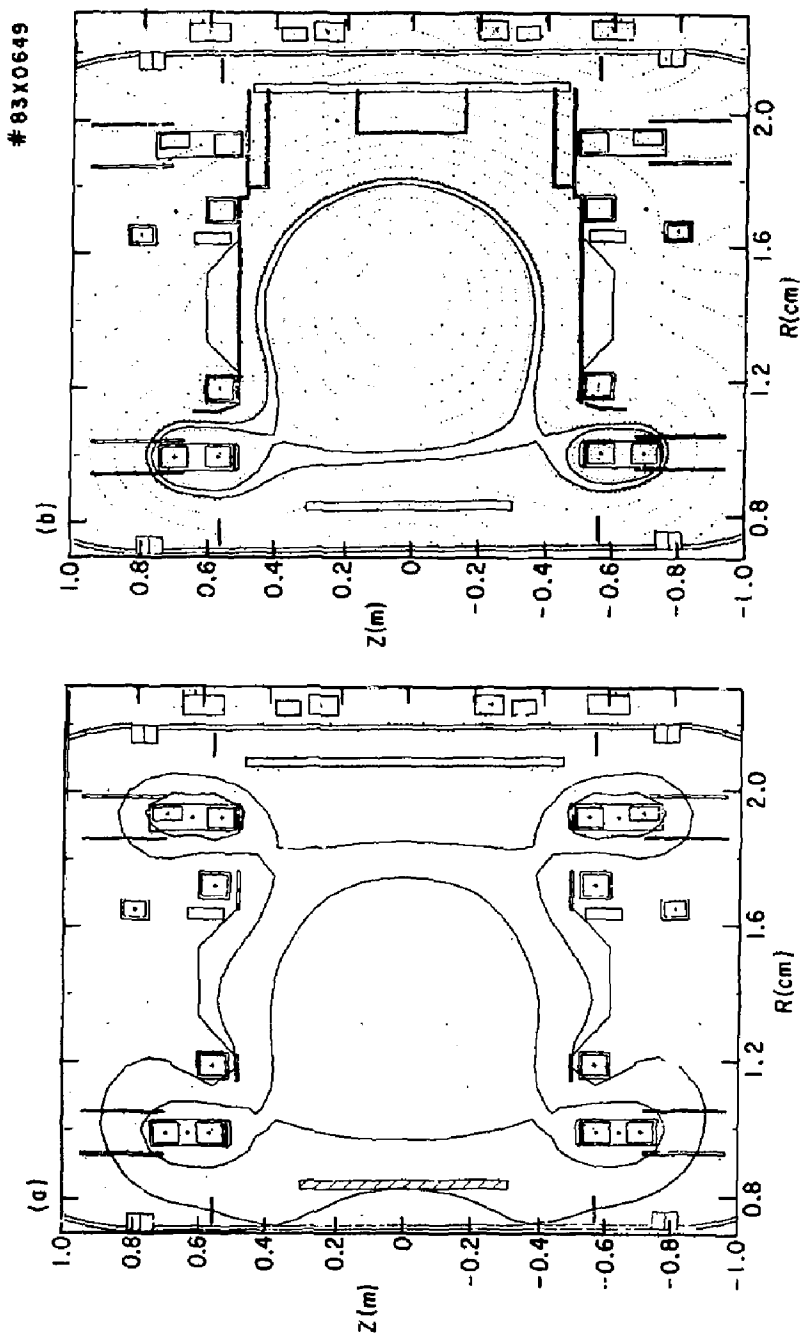

Figure 1

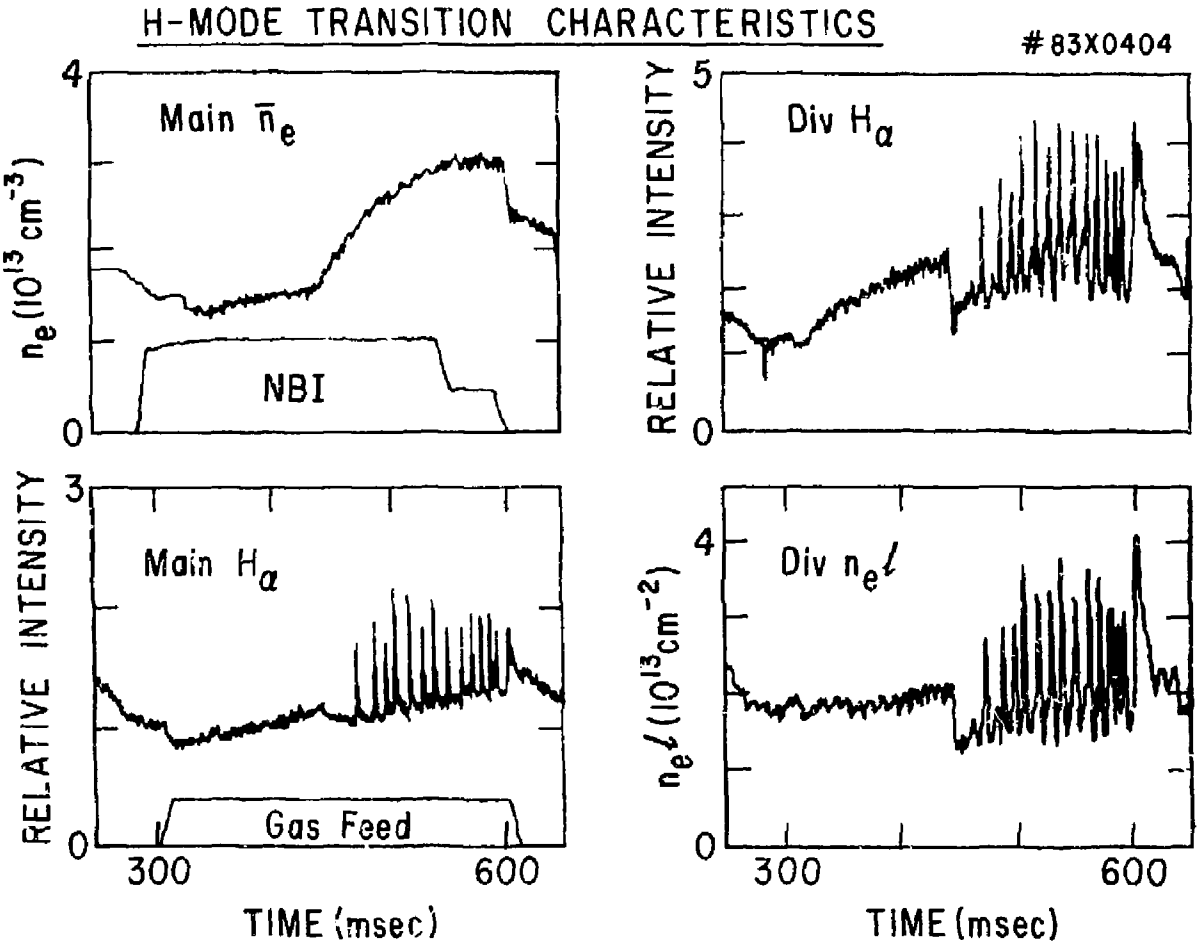
H-MODE TRANSITION CHARACTERISTICS
#83X0404
Main $\bar{n}_e$
$n_e(10^{13}\,cm^{-3})$
NBI
Div H_α
RELATIVE INTENSITY
Main H_α
Gas Feed
Div $n_e\ell$
$n_e\ell(10^{13}cm^{-2})$
300
600
TIME (msec)

Figure 2

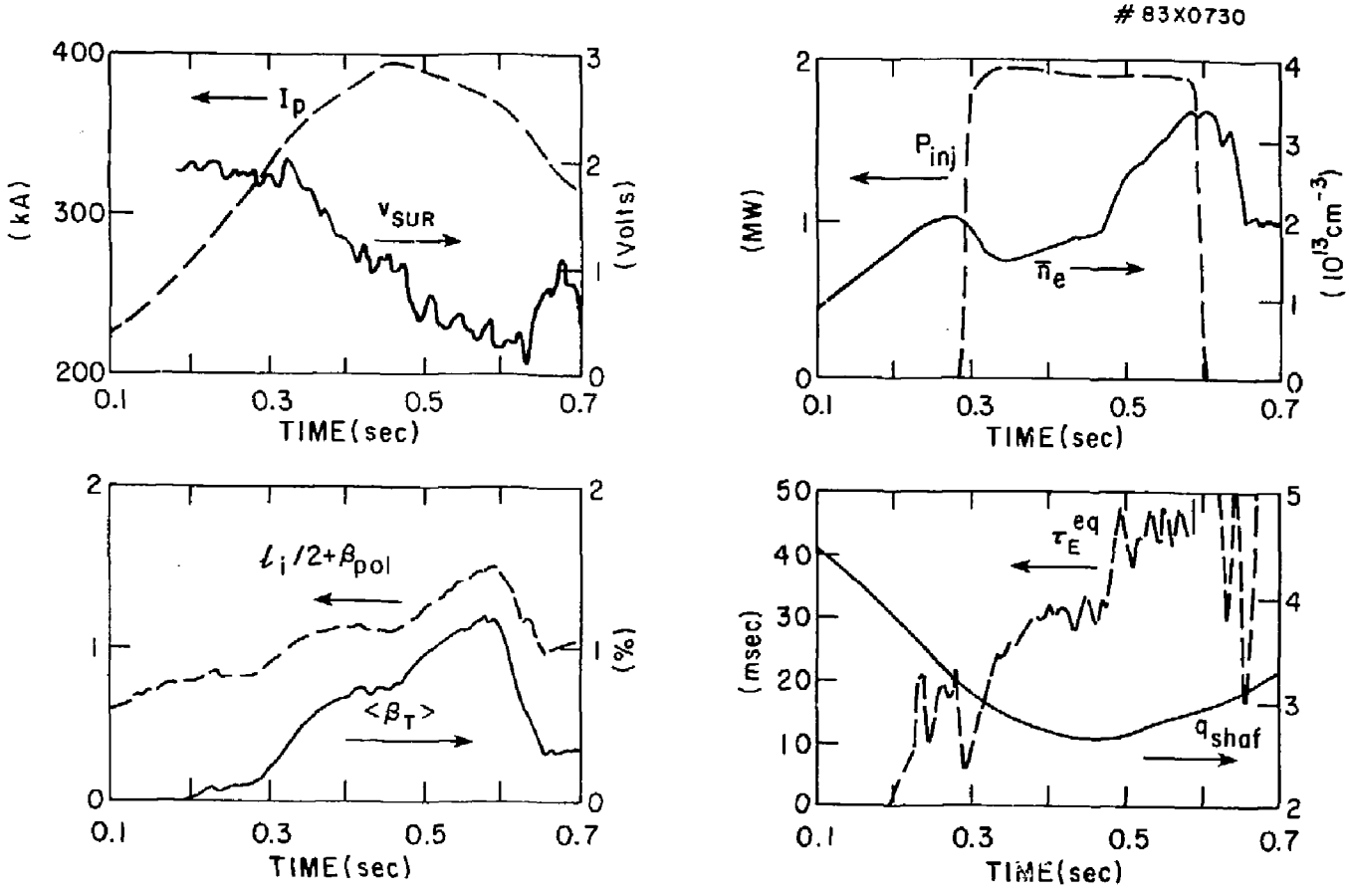
#83X0730
400
300
200
(kA)
I_p
V_{SUR}
3
2
1
0
(Volts)
0.1
0.3
0.5
0.7
TIME(sec)
2
1
0
(MW)
P_{inj}
$\bar{n}_e$
4
3
2
1
0
$(10^{13}cm^{-3})$
$\ell_i/2+\beta_{pol}$
$<\beta_T>$
(%)
50
40
30
20
10
0
(msec)
τ_E^{eq}
q_{shaf}
5
4
3
2

Figure 3

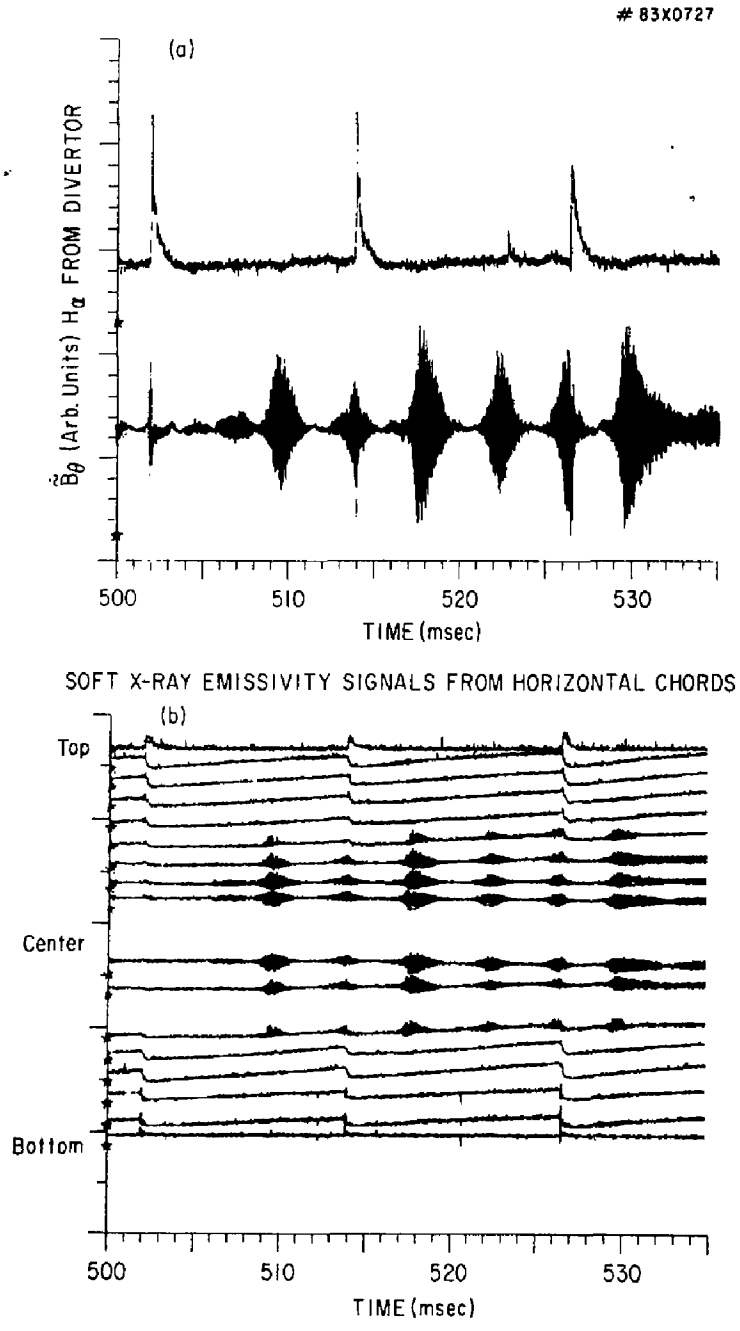
83X0727
(a)
$\tilde{B}_\theta$ (Arb. Units) H_α FROM DIVERTOR
500
510
520
530
TIME (msec)
SOFT X-RAY EMISSIVITY SIGNALS FROM HORIZONTAL CHORDS
(b)
Top
Center
Bottom
500
510
520
530
TIME (msec)

Figure 4

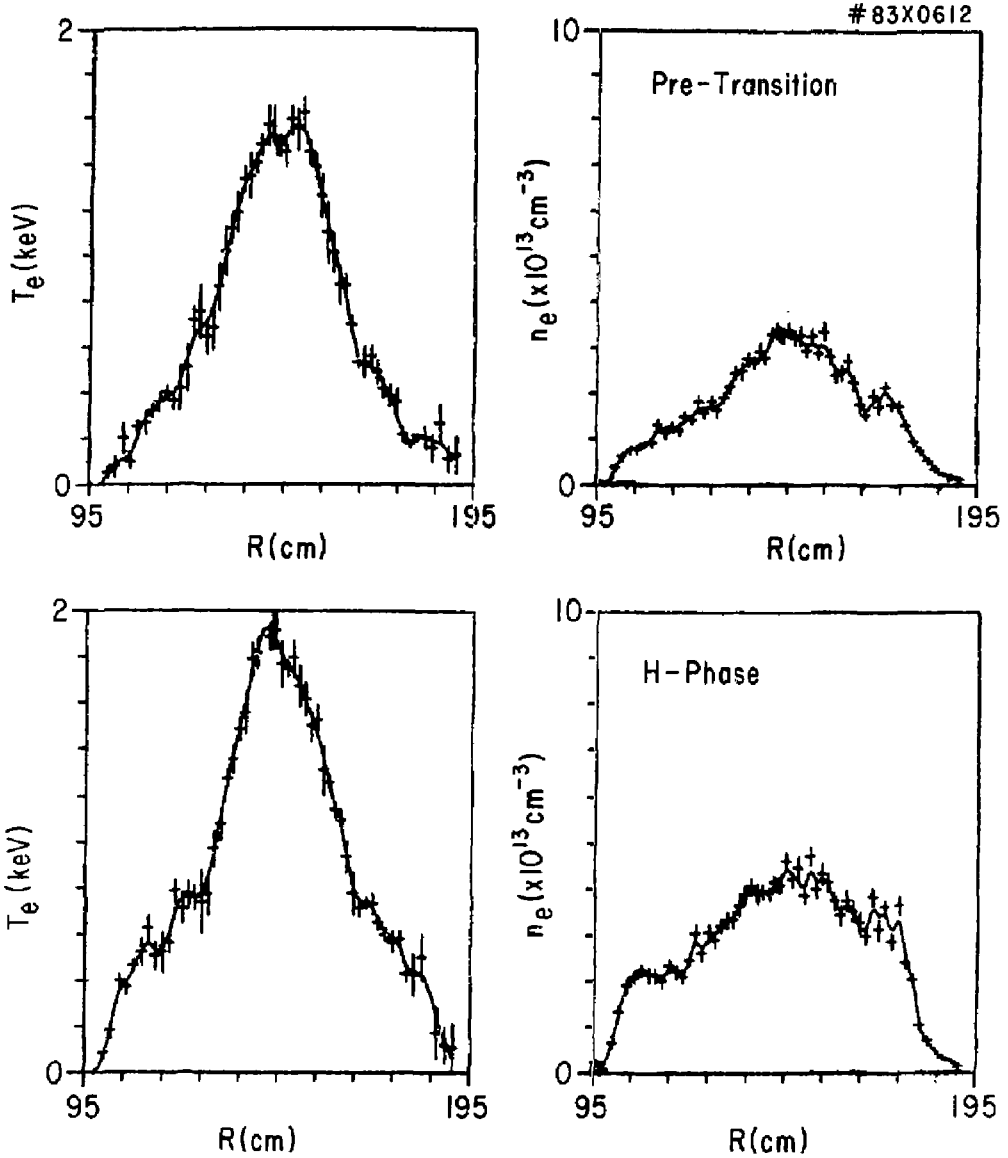
#83X0612
Pre-Transition
H-Phase
T_e(keV)
n_e(x10^{13}cm^{-3})
R(cm)
2
0
10
95
195

Figure 5

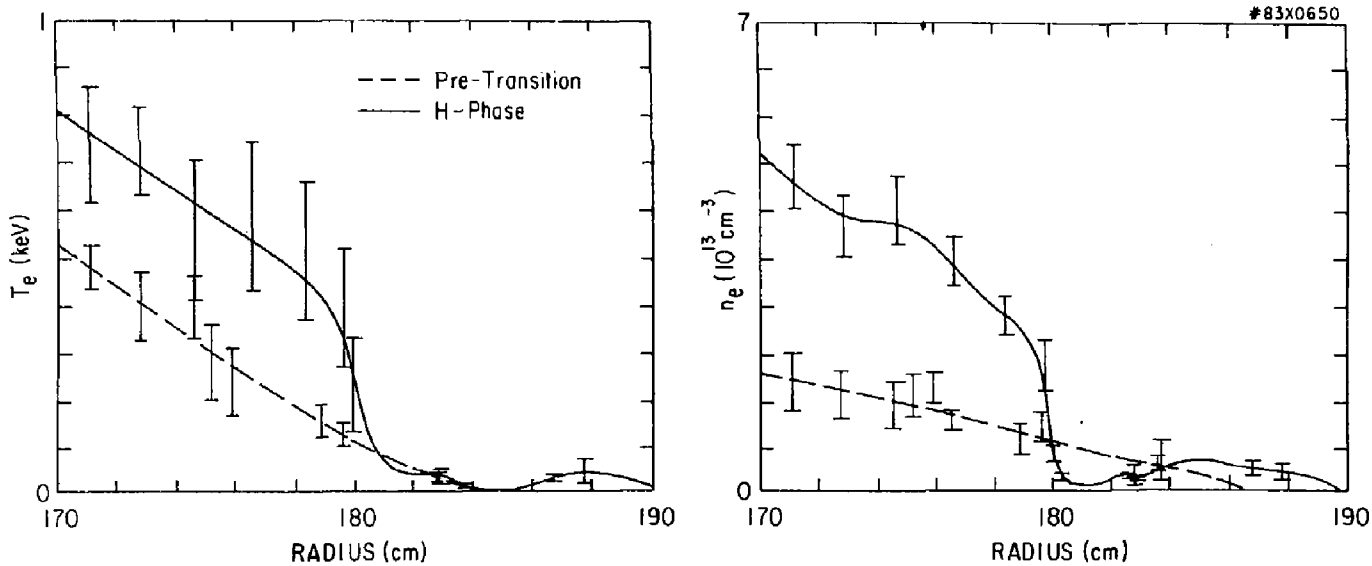
#83X0650
Pre-Transition
H-Phase
T_e (keV)
n_e (10^{13} cm^{-3})
RADIUS (cm)
RADIUS (cm)
0
1
7
170
180
190

Figure 6

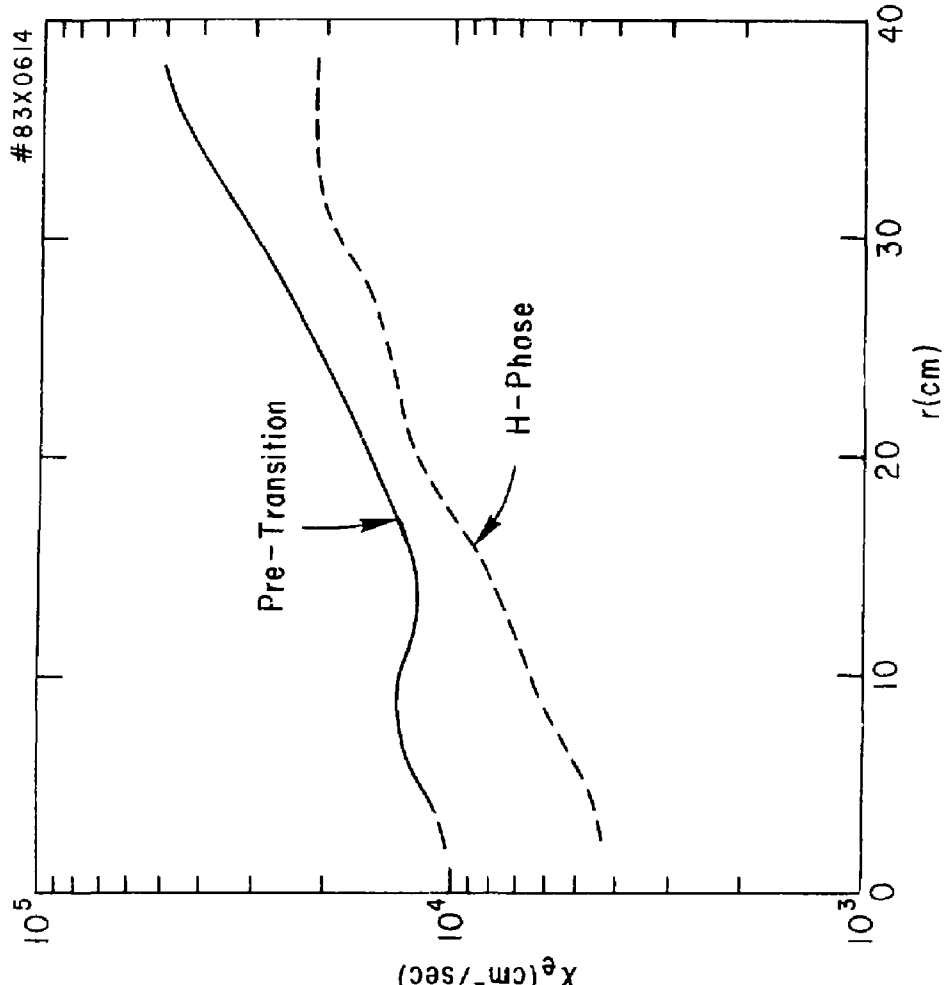
#83X0614
Pre-Transition
H-Phase
$\chi_e(cm^2/sec)$
10^5
10^4
10^3
0
10
20
30
40
r(cm)

Figure 7

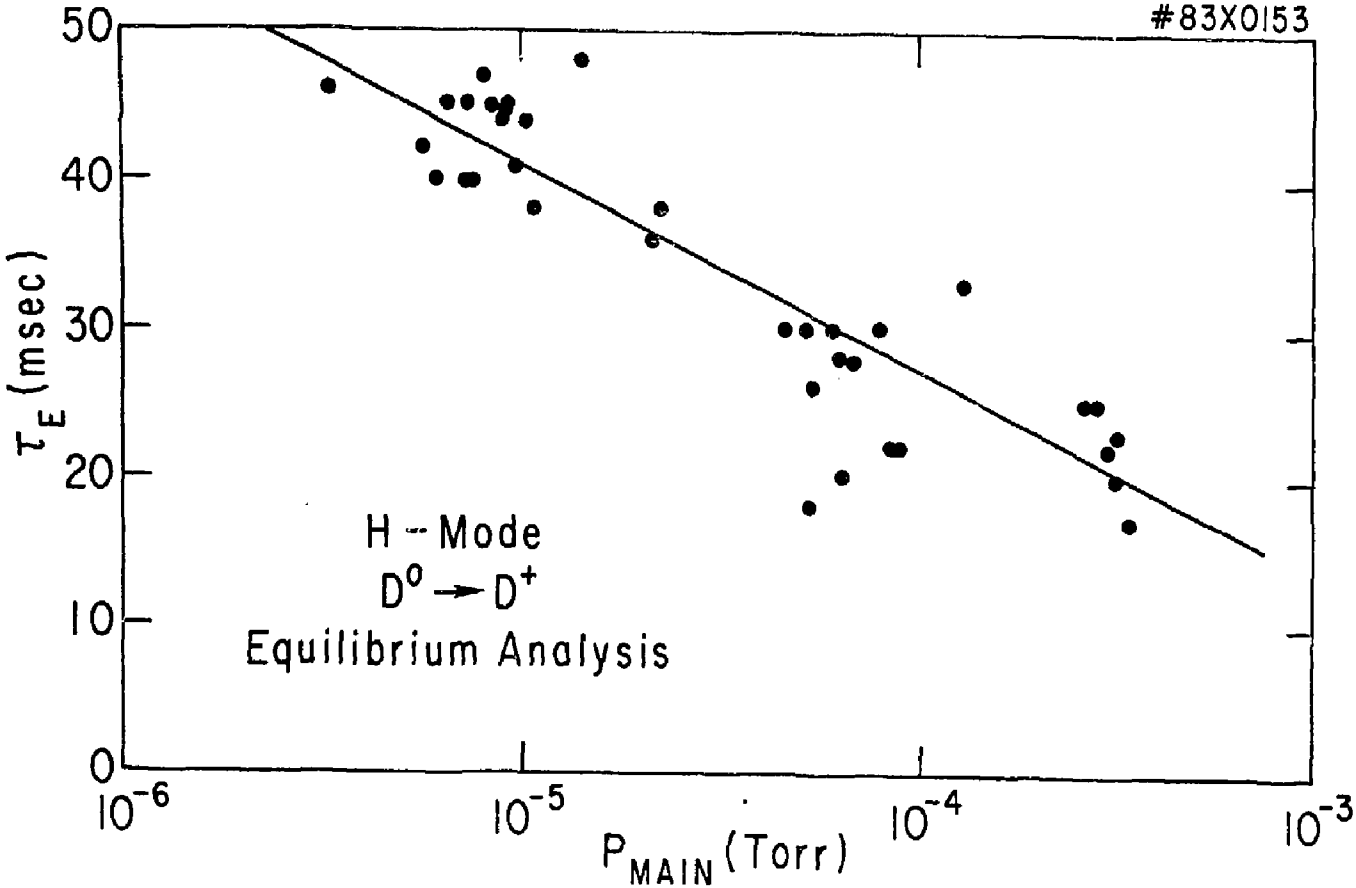
#83X0153
50
40
30
20
10
0
τ_E (msec)
H - Mode
$D^0 \rightarrow D^+$
Equilibrium Analysis
10^{-6}
10^{-5}
10^{-4}
10^{-3}
P_{MAIN} (Torr)

Figure 8

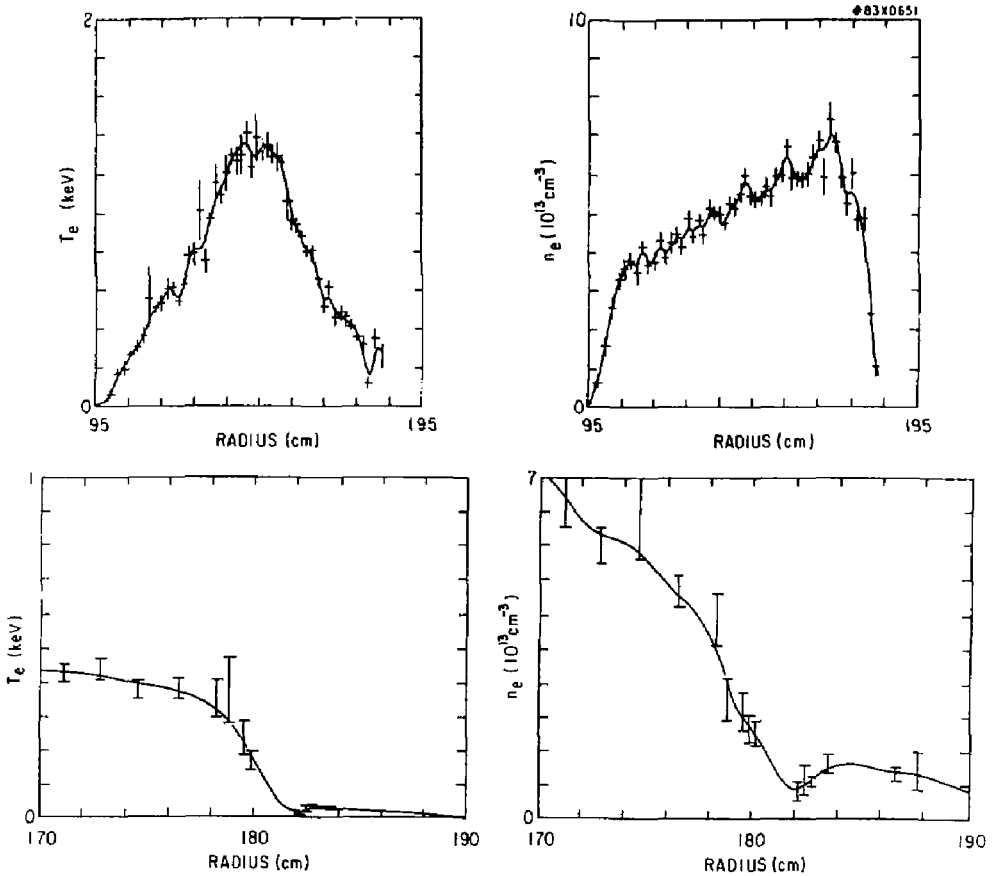
#83X0651
2
0
T_e (keV)
95
195
RADIUS (cm)
10
0
n_e (10^{13}cm^{-3})
95
195
RADIUS (cm)
1
0
T_e (keV)
170
180
190
RADIUS (cm)
7
0
n_e (10^{13}cm^{-3})
170
180
190
RADIUS (cm)

Figure 9

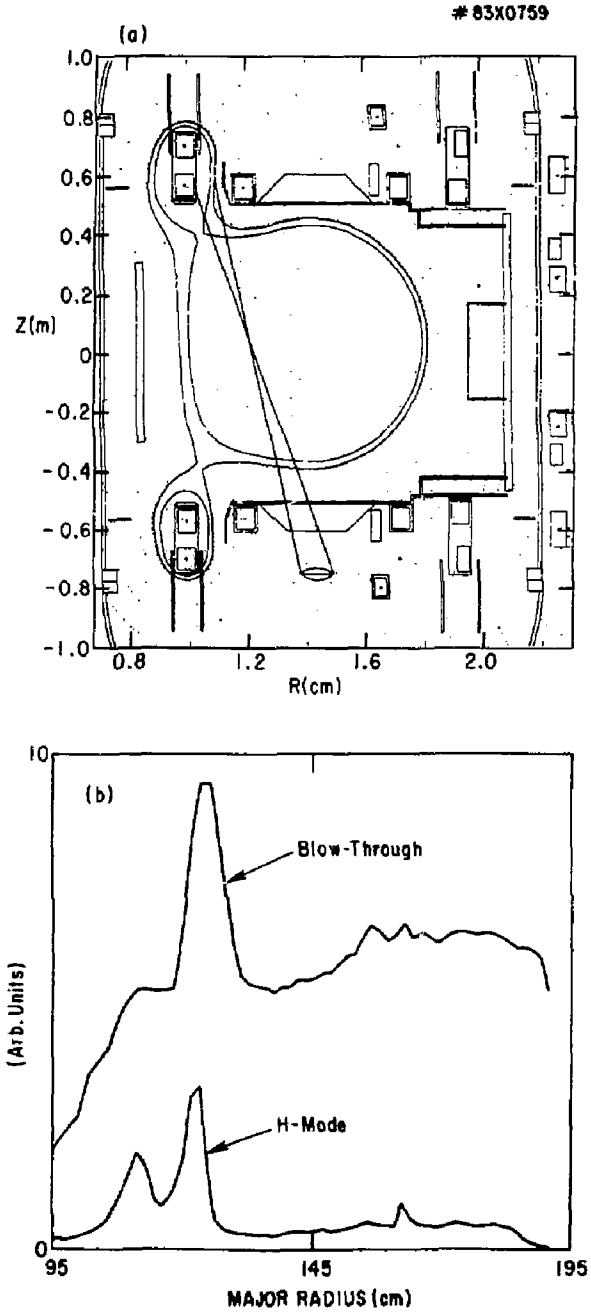
#83X0759
(a)
1.0
0.8
0.6
0.4
0.2
Z(m)
0
-0.2
-0.4
-0.6
-0.8
-1.0
0.8
1.2
1.6
2.0
R(cm)
10
(b)
Blow-Through
H-Mode
(Arb. Units)
0
95
145
195
MAJOR RADIUS (cm)

Figure 10

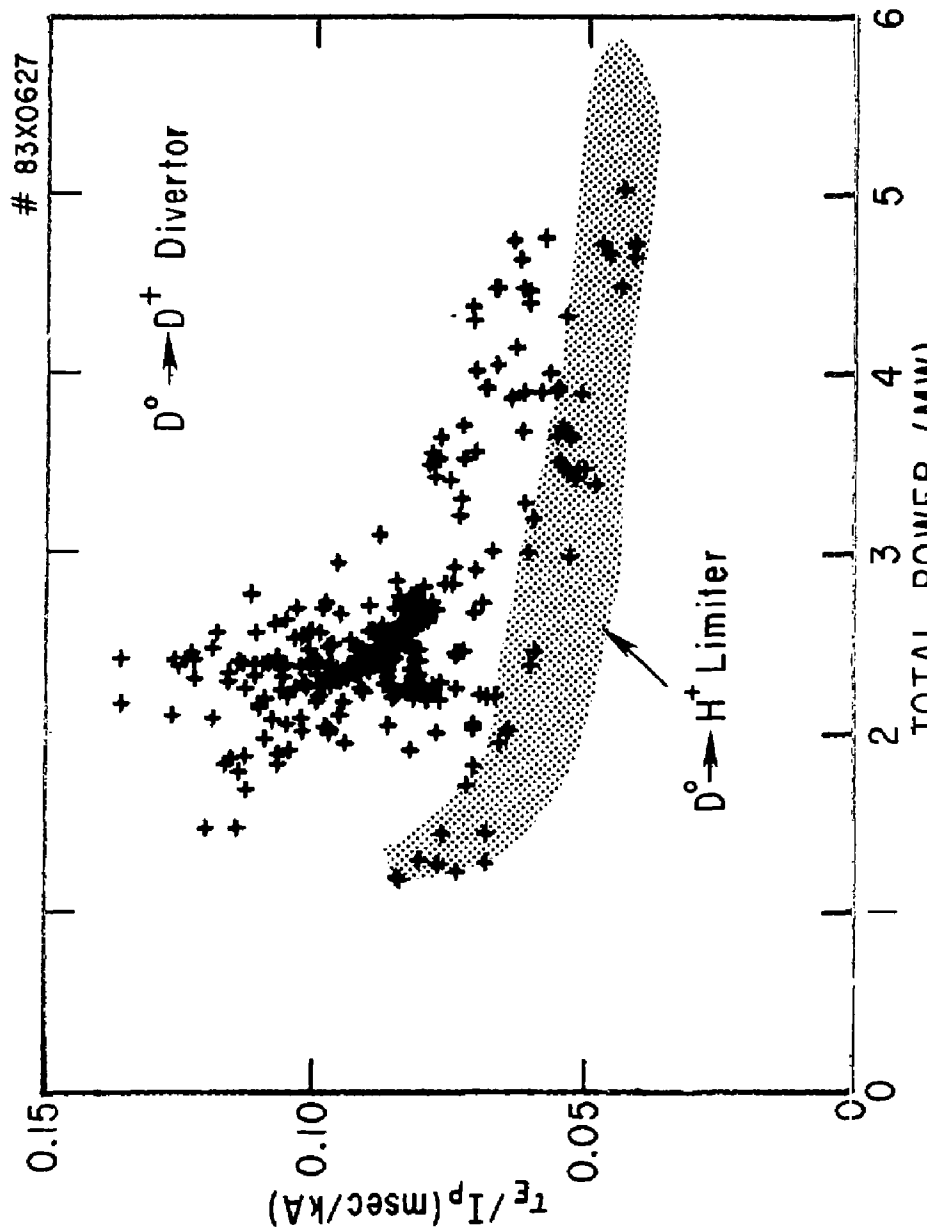
83X0627
D° → D⁺ Divertor
D° → H⁺ Limiter
τ_E/I_p (msec/kA)
0.15
0.10
0.05
0
1
2
3
4
5
6
TOTAL POWER (MW)

Figure 11

EXTERNAL DISTRIBUTION IN ADDITION TO TIC UC-20

Plasma Res Lab, Austra Nat'l Univ, AUSTRALIA
Dr. Frank J. Paoloni, Univ of Wollongong, AUSTRALIA
Prof. I.R. Jones, Flinders Univ., AUSTRALIA
Prof. M.H. Brennan, Univ Sydney, AUSTRALIA
Prof. F. Cap, Inst Theo Phys, AUSTRIA
Prof. Frank Verheest, Inst theoretische, BELGIUM
Dr. D. Palumbo, Dg XII Fusion Prog, BELGIUM
Ecole Royale Militaire, Lab de Phys Plasmas, BELGIUM
Dr. P.H. Sakanaka, Univ Estadual, BRAZIL
Dr. C.R. James, Univ of Alberta, CANADA
Prof. J. Teichmann, Univ of Montreal, CANADA
Dr. H.M. Skarsgard, Univ of Saskatchewan, CANADA
Prof. S.R. Sreenivasan, University of Calgary, CANADA
Prof. Tudor W. Johnston, INRS-Energie, CANADA
Dr. Hannes Barnard, Univ British Columbia, CANADA
Dr. M.P. Bachynski, MPB Technologies, Inc., CANADA
Zhengwu Li, SW Inst Physics, CHINA
Library, Tsing Hua University, CHINA
Librarian, Institute of Physics, CHINA
Inst Plasma Phys, Academia Sinica, CHINA
Dr. Peter Lukac, Komenskeho Univ, CZECHOSLOVAKIA
The Librarian, Culham Laboratory, ENGLAND
Prof. Schatzman, Observatoire de Nice, FRANCE
J. Radet, CEN-BP6, FRANCE
AM Dupas Library, AM Dupas Library, FRANCE
Dr. Tom Mual, Academy Bibliographic, HONG KONG
Preprint Library, Cent Res Inst Phys, HUNGARY
Dr. S.K. Trehan, Panjab University, INDIA
Dr. Indra, Mohan Lal Das, Banaras Hindu Univ, INDIA
Dr. L.K. Chavda, South Gujarat Univ, INDIA
Dr. R.K. Chhajlani, Var Ruchi Marg, INDIA
P. Kaw, Physical Research Lab, INDIA
Dr. Phillip Rosenau, Israel Inst Tech, ISRAEL
Prof. S. Cuperman, Tel Aviv University, ISRAEL
Prof. G. Rostagni, Univ Di Padova, ITALY
Librarian, Int'l Ctr Theo Phys, ITALY
Miss Clelia De Palo, Assoc EURATOM-CNEN, ITALY
Biblioteca, del CNR EURATOM, ITALY
Dr. H. Yamato, Toshiba Res & Dev, JAPAN
Prof. M. Yoshikawa, JAERI, Tokai Res Est, JAPAN
Prof. T. Uchida, University of Tokyo, JAPAN
Research Info Center, Nagoya University, JAPAN
Prof. Kyoji Nishikawa, Univ of Hiroshima, JAPAN
Prof. Sigeru Mori, JAERI, JAPAN
Library, Kyoto University, JAPAN
Prof. Ichiro Kawakami, Nihon Univ, JAPAN
Prof. Satoshi Itoh, Kyushu University, JAPAN
Tech Info Division, Korea Atomic Energy, KOREA
Dr. R. England, Ciudad Universitaria, MEXICO
Bibliotheek, Fom-Inst Voor Plasma, NETHERLANDS
Prof. B.S. Liley, University of Waikato, NEW ZEALAND
Dr. Suresh C. Sharma, Univ of Calabar, NIGERIA
Prof. J.A.C. Cabral, Inst Superior Tech, PORTUGAL
Dr. Octavian Petrus, AL I CUZA University, ROMANIA
Prof. M.A. Hellberg, University of Natal, SO AFRICA
Dr. Johan de Villiers, Atomic Energy Bd, SO AFRICA
Fusion Div. Library, JEN, SPAIN
Prof. Hans Wilhelmson, Chalmers Univ Tech, SWEDEN
Dr. Lennart Stenflo, University of UMEA, SWEDEN
Library, Royal Inst Tech, SWEDEN
Dr. Erik T. Karlson, Uppsala Universitet, SWEDEN
Centre de Recherchesen, Ecole Polytech Fed, SWITZERLAND
Dr. W.L. Weise, Nat'l Bur Stand, USA
Dr. W.M. Stacey, Georg Inst Tech, USA
Dr. S.T. Wu, Univ Alabama, USA
Prof. Norman L. Oleson, Univ S Florida, USA
Dr. Benjamin Ma, Iowa State Univ, USA
Prof. Magne Kristiansen, Texas Tech Univ, USA
Dr. Raymond Askew, Auburn Univ, USA
Dr. V.T. Tolok, Kharkov Phys Tech Ins, USSR
Dr. D.D. Ryutov, Siberian Acad Sci, USSR
Dr. G.A. Eliseev, Kurchatov Institute, USSR
Dr. V.A. Glukhikh, Inst Electro-Physical, USSR
Institute Gen. Physics, USSR
Prof. T.J. Boyd, Univ College N Wales, WALES
Dr. K. Schindler, Ruhr Universitat, W. GERMANY
Nuclear Res Estab, Julich Ltd, W. GERMANY
Librarian, Max-Planck Institut, W. GERMANY
Dr. H.J. Kaeppler, University Stuttgart, W. GERMANY
Bibliothek, Inst Plasmaforschung, W. GERMANY